Supporting information

Assembling Fe$_4$ Single Molecule Magnets on a TiO$_2$ monolayer

Andrea Luigi Sorrentino,[a,b] Lorenzo Poggini,[b,c]* Giulia Serrano,[a,b] Giuseppe Cucinotta,[b] Brunetto Cortigiani,[b] Luigi Malavolti,[d] Francesca Parenti,[e] Edwige Otero,[f] Marie-Anne Arrio,[g] Philippe Sainctavit,[f,g] Andrea Caneschi,[a] Andrea Cornia,[e] Roberta Sessoli [b,c] and Matteo Mannini.[b]*

[a.] *Department of Industrial Engineering - DIEF - and INSTM Research Unit, University of Florence, Via Santa Marta 3, 50139 Florence, Italy.*

[b.] *Department of Chemistry "U. Schiff" - DICUS - and INSTM Research Unit, University of Florence, Via della Lastruccia 3-13, 50019 Sesto Fiorentino (FI), Italy.*

[c.] *Institute for Chemistry of Organo-Metallic Compounds (ICCOM-CNR), Via Madonna del Piano, 50019 Sesto Fiorentino (FI), Italy.*

[d.] *Max Planck Institute for Solid State Research, Heisenbergstr. 1, 70569 Stuttgart, Germany.*

[e.] *Department of Chemical and Geological Sciences and INSTM Research Unit, University of Modena and Reggio Emilia, Via G. Campi 103, 41125 Modena, Italy.*

[f.] *Synchrotron-SOLEIL, L'Orme des Merisiers, 91192 Saint-Aubin, France.*

[g.] *CNRS UMR7590, Institut de Minéralogie, de Physique des Matériaux et de Cosmochimie (IMPMC), Sorbonne Université/MNHN, 4 place Jussieu, 75252 Paris Cedex 5, France.*

S1. XPS and LEED characterizations

The XPS spectrum acquired in the O 1s region shows three components (Figure S1): the main peak located at 530.1 eV (light blue) corresponds to oxygen atoms bound to Ti^{IV} atoms in the TiO_2 structure, and the peak at 531.0 eV (violet) is attributed to oxygen bound to Ti^{III} species. Finally, the peak evidenced at 532.4 eV (green filled) is due to small traces of H_2O (or OH groups) on the surface of the TiO_2 film.[1]
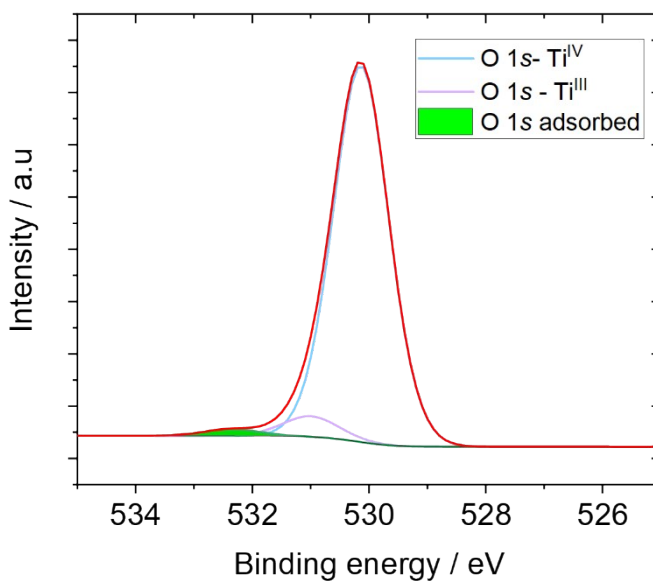

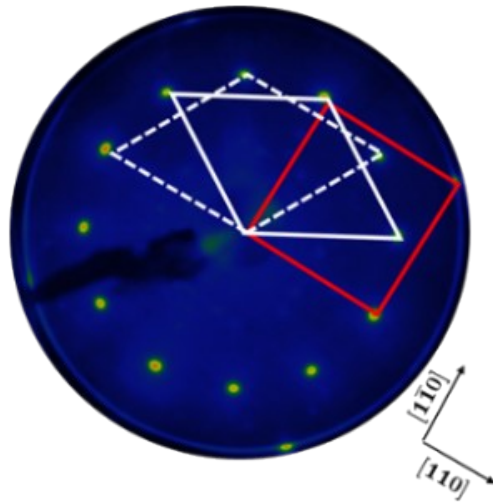**Figure S1**- XPS spectrum of TiO_2/Cu in the O 1s region.

Figure S2- LEED pattern that shows the quasi-hexagonal (QH) structure of the TiO$_2$ film (white domains) on Cu(001) (surface unit cell marked with a red square). The LEED pattern presents two domains rotated by 30 degrees with respect to each other, that are marked with white cells. The domains have been evaluated with respect to the (1 × 1) unit cell of the Cu(001) surface (red square). The absence of other spots in the pattern confirms the exclusive presence of the QH structure.
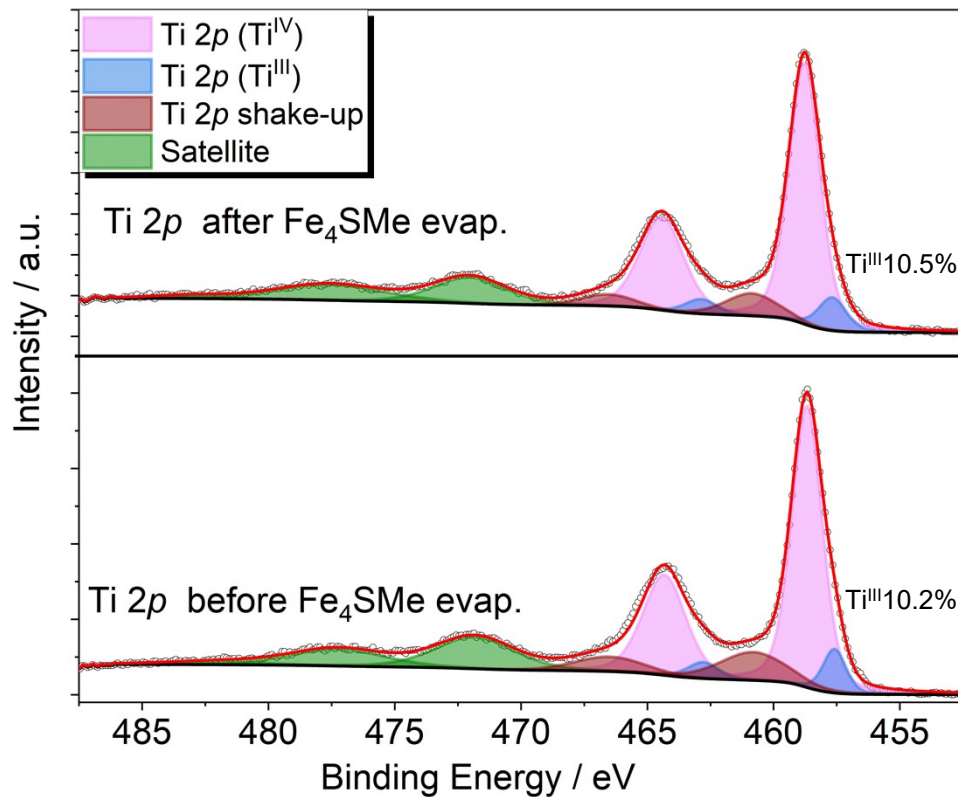
Figure S3- XPS spectra in the Ti 2p region before (bottom panel) and after (top panel) deposition of Fe$_4$SMe molecules on the TiO$_2$/Cu surface.

Table S1- Semi-quantitative analysis of the Ti^{III} and Ti^{IV} contributions to the Ti 2p region before and after deposition of Fe$_4$SMe molecules on the TiO$_2$/Cu surface.

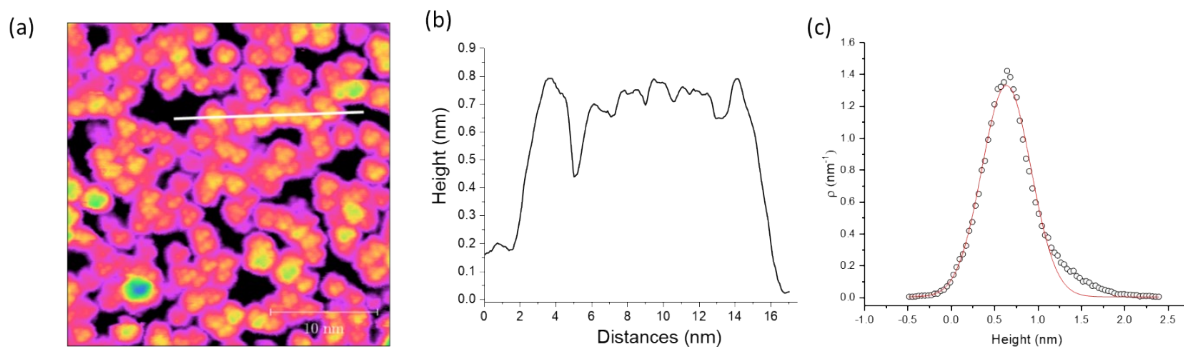|	TiO$_2$-QH	1ML Fe$_4$SMe on TiO$_2$-QH
Ti^{IV}	89.5%	89.8%
Ti^{III}	10.5%	10.2%

S2. STM Characterization

Figure S4 (a) STM image used for the estimation of the height and height distribution of Fe$_4$SMe molecules on TiO$_2$/Cu surface. (b) Height profile along the white line in panel (a). (c) Height distribution over the whole image in panel (a).
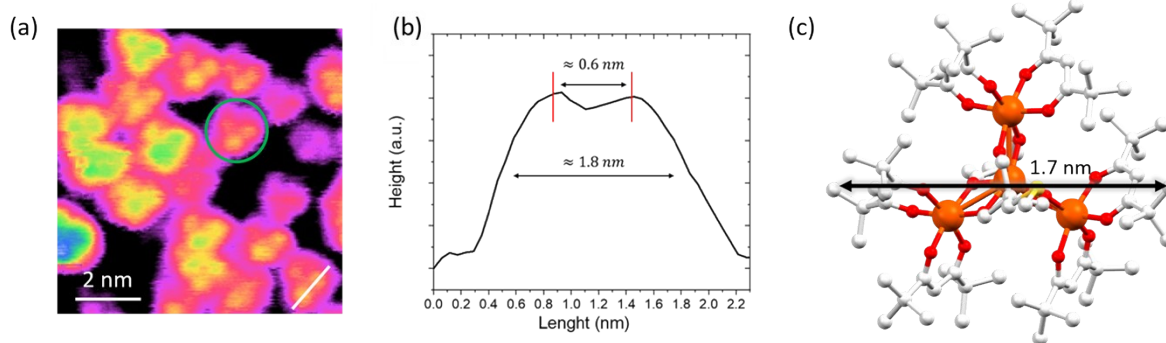

Figure S5 (a) Magnification of the STM images reported in Figure 2 and used to determine the lateral dimension of molecules. The green circle denotes a single molecule. (b) Height profile of a single molecule along the white line in panel (a); the red vertical lines mark the two bright dots found within

Fe$_4$SMe molecules. (c) Lateral dimension of the Fe$_4$SMe molecule from X-ray structure data.[2]

S3. XAS additional analyses

XAS has been also performed at the Ti L$_{2,3}$ edges to confirm the QH structure of the TiO$_2$ monolayer deposited on Cu (**Figure S6**). The L$_{2,3}$ spectrum has four main peaks, as expected, at 458.5 and 460.1 eV for the L$_3$ edge, and at 463.8 and 466.1 eV for the L$_2$ edge. The peaks result from the crystal field splitting of the 3d band into the t$_{2g}$ and e$_g$ bands.[3–5] The signal shape and separation between t$_{2g}$ and e$_g$ peaks (about 1.6 eV at the L$_3$ edge) are similar to those reported in the literature for a QH structure growth on a Ni(110) metal surface.[6] This is a further confirmation that there are no other phases on the surface and that TiO$_2$/Cu maintains the QH structure upon sublimation of the Fe$_4$SMe molecules.
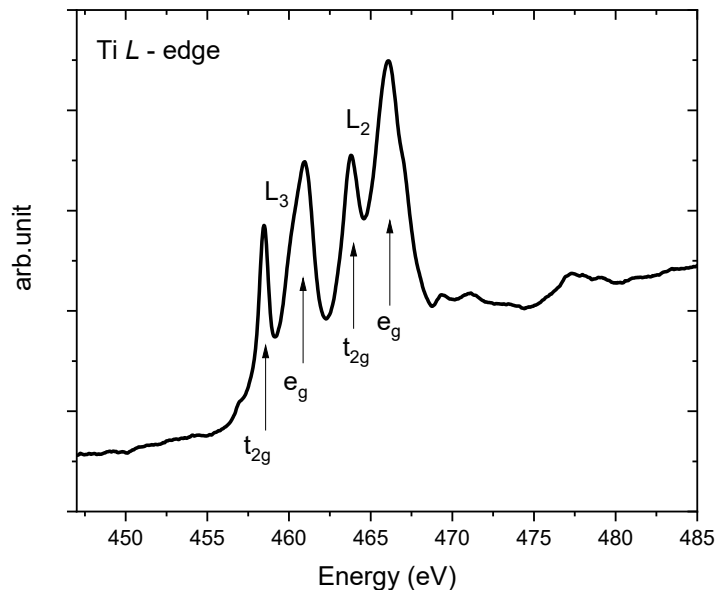
Figure S6. XAS spectrum at the Ti $L_{2,3}$ edge acquired after sublimation of the Fe_4SMe molecules on the TiO_2/Cu substrate. The spectrum was collected at a temperature of 220 mK with a magnetic field of 30 kOe at normal incidence.

S4. LFM calculations

Fe $L_{2,3}$-edges XAS and XMCD spectra are analyzed by performing Ligand Field Multiplet (LFM) calculations using Quanty (http://www.quanty.org/).[7] The symmetry is approximated as C_{3v}, following our previous work,[8] with the crystal field parameters set as follows: 10Dq = 1.32, Dσ = 0, Dτ = 0.046 eV for the peripheral Fe^{III} site, and 10Dq = 1.57, Dσ = 0, Dτ = -0.018 eV for the central Fe^{III} site. Slater integrals are scaled by a factor of 0.6. For the Fe^{II}

ions, we employ simplified O_h environments with 10Dq crystal field parameters similar to those of the Fe^{III} sites: 10Dq = 1.32 eV (Dσ = 0, Dτ = 0) for the peripheral Fe^{II} site and 10Dq = 1.57 eV (Dσ = 0, Dτ = 0) for the central Fe^{II} site. The central ion ("c") is always coupled antiferromagnetically to the peripheral ones ("p"). The XAS and XMCD responses of the pristine Fe_4 molecule are then given by:

$$\sigma_{XAS}(Fe_4) = (\sigma_{XAS}(Fe_c^{III}) + 3\sigma_{XAS}(Fe_p^{III}))$$
$$\sigma_{XMCD}(Fe_4) = (-\sigma_{XMCD}(Fe_c^{III}) + 3\sigma_{XMCD}(Fe_p^{III}))$$

Similar formulae hold for (partially) reduced Fe_4 (reduced_Fe_4). The spectra of Fe_4 and reduced_Fe_4 are then linearly combined to yield the overall spectrum of the ensemble (Fe_4@TiO_2), using the following formula which applies to both XAS and XMCD responses:

$$\sigma(Fe_4@TiO_2) = (1 - \alpha) \times \sigma(Fe_4) + \alpha \times \sigma(reduced\_Fe_4)$$

The relative amounts of Fe_4 and reduced_Fe_4 depend on the number of Fe^{III} ions replaced by Fe^{II} ions (from two to four per molecule). By fitting the XAS signal we find the presence of 30% of Fe^{II} ions and 70% of Fe^{III} ions. The XMCD signal is then fitted considering that only five different cases are compatible with the presence of 30% of Fe^{II} ions, namely:

Case 1) 40% (a = 0.6) of pristine Fe_4 molecules and 60% of Fe^{II}_c+[Fe^{II}_p+2Fe^{III}_p] molecules,

Case 2) 40% (a = 0.6) of pristine Fe_4 molecules and 60% of Fe^{III}_c+[$2Fe^{II}_p$+Fe^{III}_p] molecules,

Case 3) 60% (a = 0.4) of pristine Fe_4 molecules and 40% of Fe^{II}_c+[$2Fe^{II}_p$+Fe^{III}_p] molecules,

Case 4) 60% (a = 0.4) of pristine Fe_4 molecules and 40% of Fe^{III}_c+[$3Fe^{II}_p$] molecules,

Case 5) 70% (a = 0.3) of pristine Fe_4 molecules and 30% of Fe^{II}_c+[$3Fe^{II}_p$] molecules.

Figure S7 shows the different normalized calculations with comparison to the normalized experimental spectra (normalization relative to the maximum of the XAS at L_3 edge).

The best fit is obtained for **Case 5**, i.e. 70% of pristine Fe_4 molecules and 30% of Fe^{II}_c+[$3Fe^{II}_p$] molecules. Obviously, one cannot exclude that a minority fraction of Fe^{II} ions is distributed according to **Cases 1** to **4**.
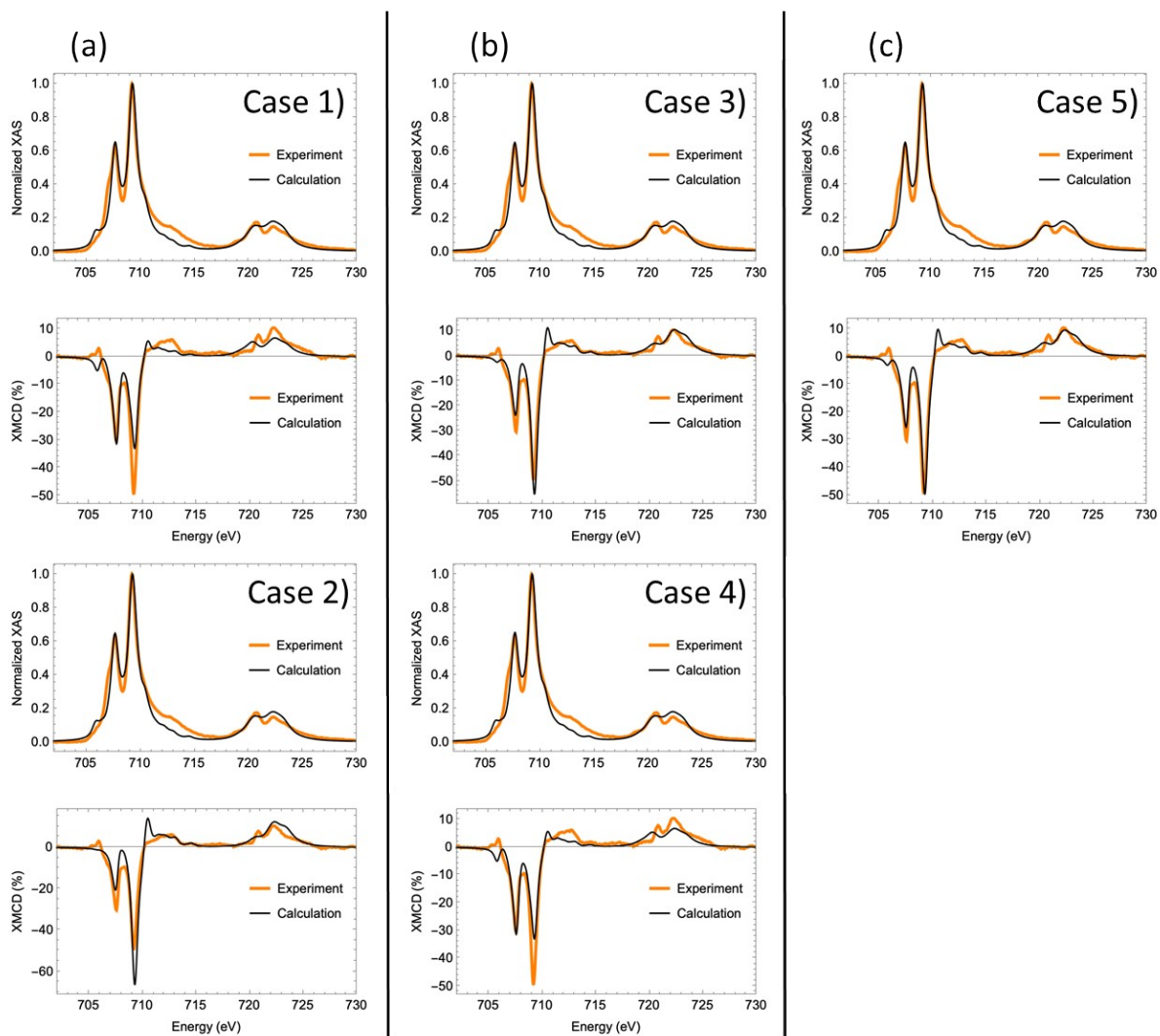
Figure S7. Normalized experimental (orange line) and calculated (black line) XAS and XMCD. The LFM calculations are for a linear combination of pristine Fe_4 molecules and (partially) reduced Fe_4 molecules containing a variable number of Fe^{II} ions, namely two in **Cases 1)** and **2)**, three in **Cases 3)** and **4)**, and four in **Case 5)**. The relative amounts of pristine Fe_4 and (partially) reduced Fe_4 are given in the text above.
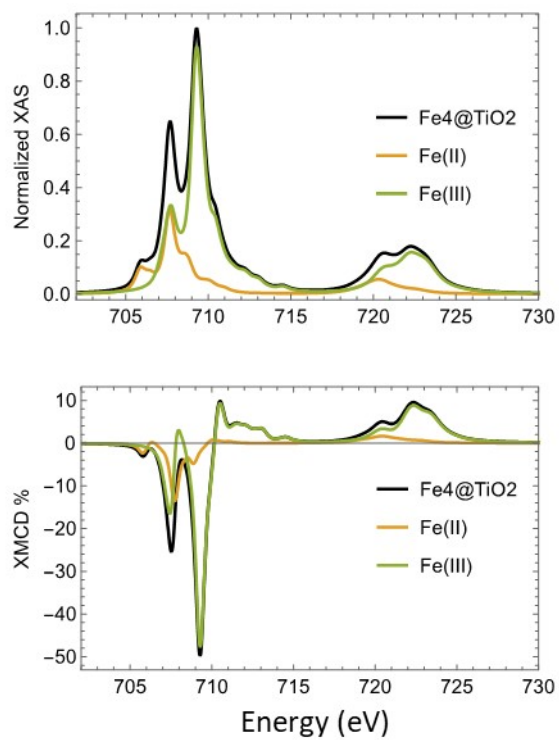
Figure S8. Normalized calculated XAS and XMCD for 70% of pristine Fe$_4$ molecules and 30% of Fe$^{II}_c$+[3Fe$^{II}_p$] molecules (**Case 5**, black line), along with the individual contributions of Fe^{II} (orange line) and Fe^{III} (green line).

References

1   A. L. Sorrentino, G. Serrano, L. Poggini, B. Cortigiani, K. E. El-Kelany, M. D'Amore, A. M. Ferrari, A. Atrei, A. Caneschi, R. Sessoli and M. Mannini, *J. Phys. Chem. C*, 2021, **125**, 10621–10630.

2   G. Serrano, L. Poggini, M. Briganti, A. L. Sorrentino, G. Cucinotta, L. Malavolti, B. Cortigiani, E. Otero, P. Sainctavit, S. Loth, F. Parenti, A.-L. L. Barra, A. Vindigni, A. Cornia, F. Totti, M. Mannini and R. Sessoli, *Nat. Mater.*, 2020, **19**, 546–551.

3   R. Singh, M. Gupta, D. M. Phase and S. K. Mukherjee, *Mater. Res. Express*, 2019, **6**, 116449.

4   S. C. Chen, K. Y. Sung, W. Y. Tzeng, K. H. Wu, J. Y. Juang, T. M. Uen, C. W. Luo, J. Y. Lin, T. Kobayashi and H. C. Kuo, *J. Phys. D. Appl. Phys.*, 2013, **46**, 075002.

5   K. Płacheta, A. Kot, J. Banas-Gac, M. Zając, M. Sikora, M. Radecka and K. Zakrzewska, *Appl. Surf. Sci.*, 2023, **608**, 155046.

6   A. C. Papageorgiou, G. Cabailh, Q. Chen, A. Resta, E. Lundgren, J. N. Andersen and G. Thornton, *J. Phys. Chem. C*, 2007, **111**, 7704–7710.

7   M. W. Haverkort, M. Zwierzycki and O. K. Andersen, *Phys. Rev. B*, 2012, **85**, 165113.

8   M. Mannini, F. Pineider, C. Danieli, F. Totti, L. Sorace, P. Sainctavit, M.-A. Arrio, E. Otero, L. Joly, J. C. Cezar, A. Cornia and R. Sessoli, *Nature*, 2010, **468**, 417–421.